QED Compton scattering in high-energy electron-proton collisions

A. Courau
Laboratoire de l'Accélérateur Linéaire, Institut National de Physique Nucléaire et de Physique de Particules, Centre National de la Recherche Scientifique, Université de Paris-Sud, F-91405 Orsay CEDEX, France

P. Kessler
Collège de France, Institut National de Physique Nucléaire et de Physique de Particules, Centre National de la Recherche Scientifique, Laboratoire de Physique Corpusculaire, 11 place Marcelin Berthelot, F-75231 Paris CEDEX 05, France

(Received 14 February 1992)

We here provide exact analytic formulas and therefrom derive a Monte Carlo program without approximations, for QED Compton events in the reaction $ep \to e\gamma X$ produced in head-on ep collisions. Those events correspond to final states with an electron and a photon, nearly coplanar, observed at a finite angle within the detector. The process here studied can be used, at high-energy electron-proton colliders, for various purposes: measurement of the luminosity; electromagnetic calibration of detectors; search for an e^*; and finally, determination of the photon content of the proton.

PACS number(s): 13.60.Fz, 12.20.Ds, 29.20.Mr

I. INTRODUCTION

In a previous paper [1], we had suggested using QED Compton scattering, which is one of the processes contributing to the reaction $ep \to e\gamma X$ produced in head-on collisions, at high-energy electron-proton colliders, for various purposes: the measurement of luminosity, the electromagnetic calibration of detectors, and the search for an excited electron e^*. In that work we assumed that the outgoing electron and photon would be measured at finite angles, with their total transverse momentum limited to a value close to zero; this assumption allowed us to isolate the QED Compton contribution, and also to perform a simplified and rough calculation, using the equivalent-photon approximation for the proton, and in addition by treating the latter like a pure Dirac particle.

In this paper we shall improve our calculation of the QED Compton process by not using any approximation in the Feynman graph computation and by introducing a more precise expression of the photon content of the proton. Unavoidably that expression will remain model dependent to some extent (mainly as far as its inelastic part is concerned). Let us notice that the determination of the exact photon content of the photon would actually be an additional purpose of the experiment here suggested [2].

Before we start presenting our formalism, let us specify briefly, and somewhat schematically, what is meant by QED Compton scattering and how it is selected from the reaction $ep \to e\gamma X$.

For both Feynman diagrams of Fig. 1, the corresponding amplitude contains the denominator $(q_1^2 - m_e^2)q_2^2$ $[(q_1'^2 - m_e^2)q_2^2]$. From there it results that the dominant contribution stems from the configuration where both q_1^2 $(q_1'^2)$ and q_2^2 stay close to zero. This configuration corresponds to the so-called *bremsstrahlung process*. It involves quite large counting rates but, in order to be measured, requires a specific small-angle detector [3].

Looking for particles within a finite-angle detector requires that at least one of the two q^2's takes finite values; the cross section will then be dominated by the range where the other q^2 stays close to zero. One may thus consider, in that case, two different configurations giving rise to counting rates that are still relatively significant.

(i) q_1^2 $(q_1'^2) \simeq 0$, q_2^2 finite: the final photon is emitted along the incident (final) electron line; in the detector one observes the outgoing electron (nearly collinear, and therefore indistinguishable, electron and photon) and at least part of the outgoing hadronic system. That configuration corresponds to the so-called *radiative correction* to electron-proton scattering [4].

(ii) $q_2'^2 \simeq 0$, q_1^2 $(q_1'^2)$ finite: the hadronic system goes straightforwardly along the incident-proton line, and what we observe in the detector is the electron and the photon, with their total transverse momentum close to zero. This configuration involves what we are calling the *QED Compton process*, initiated by quasireal photons. That process will thus be selected by performing a cut on the total transverse momentum of the outgoing electron and photon or, more or less equivalently, on the aco-

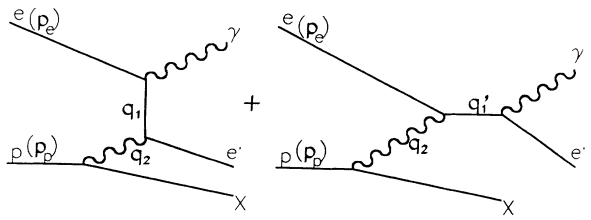

FIG. 1. Feynman diagrams here considered for $ep \to e\gamma X$.

planarity of the electron-photon system. Such a cut will also ensure that we can safely neglect contributions from other reaction mechanisms, in particular from Feynman diagrams (not shown in Fig. 1) where the outgoing photon is emitted at the hadron vertex.

In Sec. II we shall present the full and exact calculation of the Feynman graphs of Fig. 1. Section III contains the description of a Monte Carlo program for the generation of QED Compton events and some predictions for distributions of various parameters in an experiment of that type, assumed to be performed at the DESY *ep* collider HERA. We shall finish with a brief conclusion, where we shall discuss further extension of our work.

II. EXACT ANALYTIC CALCULATION

We start with the exact factorization formula, based on helicity, for the process shown in Fig. 1:

$$\frac{d^4\sigma^{pe\to e\gamma X}}{dx\,dx_\gamma dQ^2 d\Omega^*}=f^T_{\gamma^*/p}(x,x_\gamma,Q^2)\left[\frac{d\sigma}{d\Omega^*}\right]^T+f^L_{\gamma^*/p}(x,x_\gamma,Q^2)\left[\frac{d\sigma}{d\Omega^*}\right]^L \tag{1}$$

with

$$\left[\frac{d\sigma}{d\Omega^*}\right]^T=\frac{d\sigma_T}{d\Omega^*}+\epsilon\frac{d\sigma_L}{d\Omega^*}+\sqrt{2\epsilon(1+\epsilon)}\frac{d\sigma_{TL}}{d\Omega^*}\cos\varphi^*+\epsilon\frac{d\sigma_{TT}}{d\Omega^*}\cos 2\varphi^* \tag{2}$$

$$\left[\frac{d\sigma}{d\Omega^*}\right]^L=\frac{d\sigma_T}{d\Omega^*}+\frac{1+\epsilon}{2\epsilon}\frac{d\sigma_L}{d\Omega^*}+\left[2\frac{1+\epsilon}{\epsilon}\right]^{1/2}\frac{d\sigma_{TL}}{d\Omega^*}\cos\varphi^*+\frac{d\sigma_{TT}}{d\Omega^*}\cos 2\varphi^* \tag{3}$$

where the upper subscript (T,L) refers to the virtual photon's polarization (transverse or longitudinal) at the hadron vertex, while the lower one (T,L,TL,TT) refers to its polarization at the lepton vertex, i.e., defines the transverse cross section, the longitudinal cross section, the transverse-longitudinal interference term and the transverse-transverse interference term of the virtual Compton scattering process $\gamma^* e\to\gamma e$.

In formula (1) the "virtual photon spectra" $f^{T,L}$ are given by

$$f^T_{\gamma^*/p}=\frac{1-x}{4\pi^3 x x_\gamma}g^T(x,x_\gamma,Q^2)\sigma^T_{\gamma^* p}\ , \tag{4}$$

$$f^L_{\gamma^*/p}=\frac{1-x}{4\pi^3 x x_\gamma}g^L(x,x_\gamma,Q^2)\sigma^L_{\gamma^* p} \tag{5}$$

with

$$g^L(x,x_\gamma,Q^2)=g^T(x,x_\gamma,Q^2)-\frac{x_\gamma^2}{2x^2}=\frac{(1-x_\gamma/x)Q^2-x_\gamma^2 m_p^2}{Q^2+4x^2m_p^2} \tag{6}$$

where the variables Q^2,x,x_γ are defined as

$$Q^2=-\mathbf{q}_2^2,\quad x=\frac{-\mathbf{q}_2^2}{2\mathbf{p}_p\cdot\mathbf{q}_2}=\frac{Q^2}{m_X^2-m_p^2+Q^2}\ ,$$

$$x_\gamma=\frac{\mathbf{q}_2\cdot\mathbf{p}_e}{\mathbf{p}_p\cdot\mathbf{p}_e}=\frac{W^2+Q^2-m_e^2}{s-m_p^2-m_e^2}\simeq\frac{W^2+Q^2}{s}\ ,$$

calling m_X, m_p, m_e the respective masses of X, p, and e, and defining $W^2=(\mathbf{q}_2+\mathbf{p}_e)^2$, $s=(\mathbf{p}_p+\mathbf{p}_e)^2$. The cross sections $\sigma^{T,L}_{\gamma^* p}$ pertain to the virtual process $\gamma^* p\to X$; their expressions will be given below.

In formulas (2) and (3) the virtual photon's polarization parameter ϵ is given by $\epsilon=g^L/g^T$ [see (6)]. On the other hand, the various polarization terms for the virtual Compton scattering are given by [5]

$$d\sigma_T=\frac{\alpha^2}{W^2+Q^2}\left[\frac{W^2}{(W^2+Q^2)(1+u^*+\eta)}+\frac{(W^2+Q^2)(1+u^*)}{4W^2}+\frac{Q^2}{W^2}\frac{1-u^*}{W^2(1+u^*+\eta)}+\frac{Q^2(1-u^*)}{2(W^2+Q^2)}\right]d\Omega^*\ , \tag{7}$$

$$d\sigma_L=\frac{\alpha^2}{W^2+Q^2}\left[\frac{Q^2(1-u^*)}{W^2+Q^2}\right]d\Omega^*\ , \tag{8}$$

$$d\sigma_{TL}=\frac{\alpha^2}{W^2+Q^2}\left[\frac{QW}{2(W^2+Q^2)}\sqrt{1-u^{*2}}\left(1+\frac{Q^2}{W^2}\frac{1-u^*}{1+u^*+\eta}\right)\right]d\Omega^*\ , \tag{9}$$

$$d\sigma_{TT}=\frac{\alpha^2}{W^2+Q^2}\left[\frac{Q^2}{2(W^2+Q^2)}(1-u^*)\right]d\Omega^*\ , \tag{10}$$

where $d\Omega^*=du^*d\varphi^*$, with $u^*=\cos\theta^*$, θ^* and φ^* being the orbital and azimuthal scattering angles in the center-of-mass frame of the virtual Compton process. Finally, $\eta=2m_e^2W^2/(W^2+Q^2)^2$ (notice that we take the electron mass into account only where it is required in order to avoid a divergency in the formulas).

Now, in order to specify $\sigma^{T,L}_{\gamma^* p}$, we shall consider various separate contributions depending on the value (range) of m_X involved [6].

A. Elastic contribution: $m_X=m_p$

$$\sigma^T_{\gamma^* p}=\frac{4\pi^2\alpha}{Q^2}G_M^2(Q^2)\frac{\delta(1-x)}{1-x}\ , \tag{11}$$

$$\sigma^L_{\gamma^* p}=\frac{16\pi^2\alpha m_p^2}{Q^4}G_E^2(Q^2)\frac{\delta(1-x)}{1-x}\ , \tag{12}$$

where we use the conventional expressions of the proton's electromagnetic form factors:

$$G_E(Q^2)=\frac{G_M(Q^2)}{2.79}=(1+Q^2/Q_0^2)^{-2} \tag{13}$$

with $Q_0^2=0.71$ GeV^2.

TABLE I. Characteristics of the three resonances here considered.

	Δ	N^*	N^*
m_R (GeV)	1236	1520	1688
σ_R (μb)	550	280	220
Γ_R (GeV)	0.12	0.12	0.12
Q_R^2 (GeV^2)	2.5	3.0	3.0

B. Resonant contribution $m_p+m_\pi<m_X<1.8$ GeV

We assume that range to be essentially saturated by the contribution of the three resonances Δ (1236), N^* (1520), N^* (1688). From experimental data on electroproduction [7] we derive

$$\sigma^T=\sum_R \sigma_R \frac{m_R^2\Gamma_R^2}{(m_X^2-m_R^2)^2+m_R^2\Gamma_R^2}\left[1+\frac{Q^2}{Q_R^2}\right]^{-2} \tag{14}$$

$$\sigma^L=0 \tag{15}$$

with the values of the various parameters given in Table I.

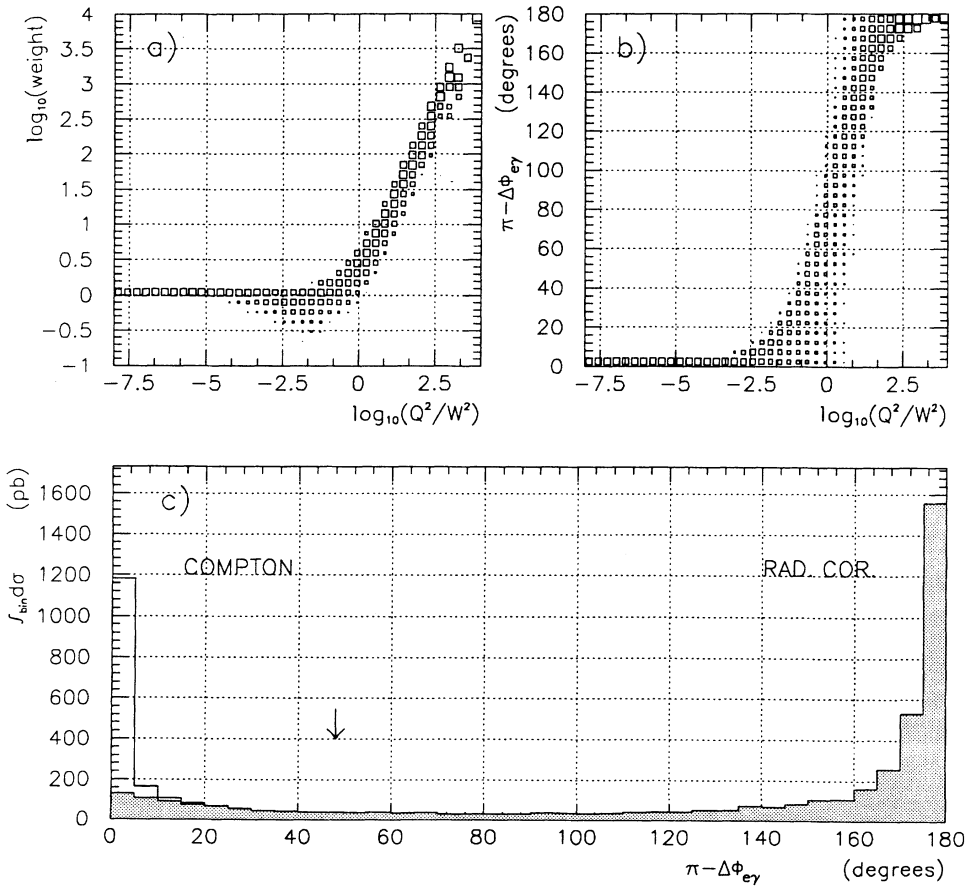

FIG. 2. (a) Correlation between Q^2/W^2 and weight (see Sec. III). (b) Correlation between Q^2/W^2 and acoplanarity angle. (c) Acoplanarity distribution; the shaded area represents the inelastic contribution. Those figures show weighted distributions computed for HERA conditions (see Sec. III) before introducing acoplanarity and P_T cuts.

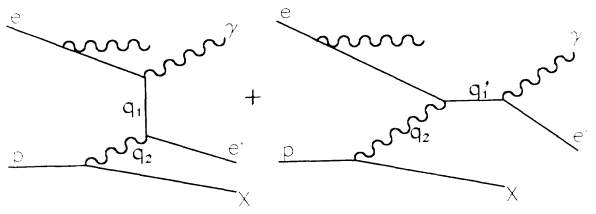

FIG. 3. Radiative correction on the incident-electron line for QED Compton events.

C. Continuum inelastic contribution: $m_X > 1.8$ GeV

(i) For large Q^2, with the assumption (justified by the quark-parton model) $\sigma_L=(Q^2/\nu^2)\sigma_T$, defining $\nu=Q^2/(2m_p x)$, we get

$$\sigma_T=\frac{4\pi^2\alpha}{(1-x)Q^2}F_2^p(x,Q^2)\ , \tag{16}$$

$$\sigma_L=\frac{4\pi^2\alpha}{(1-x)Q^2}\frac{4x^2m_p^2}{Q^2}F_2^p(x,Q^2)\ , \tag{17}$$

where $F_2^p(x,Q^2)$ is the classical proton structure function.

(ii) When Q^2 tends to zero, we are led to the well-known cross section of real-photon production:

$$\sigma_T\simeq 100\ \mu b\ ,$$

$$\sigma_L=0\ .$$

(iii) Finally we set over the full Q^2 range:

$$\sigma_T=\frac{4\pi^2\alpha}{(1-x)Q^2}F_2^p(x,Q^2)\phi(x,Q^2)\ , \tag{18}$$

$$\sigma_L=\frac{4\pi^2\alpha}{(1-x)Q^2}\frac{4x^2m_p^2}{Q^2}F_2^p(x,Q^2)\phi(x,Q^2) \tag{19}$$

where the interpolation function $\phi(x,Q^2)$ is defined as

$$\phi(x,Q^2)=\frac{Q^2\ (\mathrm{GeV}^2)}{Q^2(\mathrm{GeV}^2)+F_2^p(x,Q^2)} \tag{20}$$

noticing that x goes to zero (while x/Q^2 stays finite) with $Q^2\to 0$, and that $4\pi\alpha^2/(1\ \mathrm{GeV}^2)\simeq 100\ \mu b$.

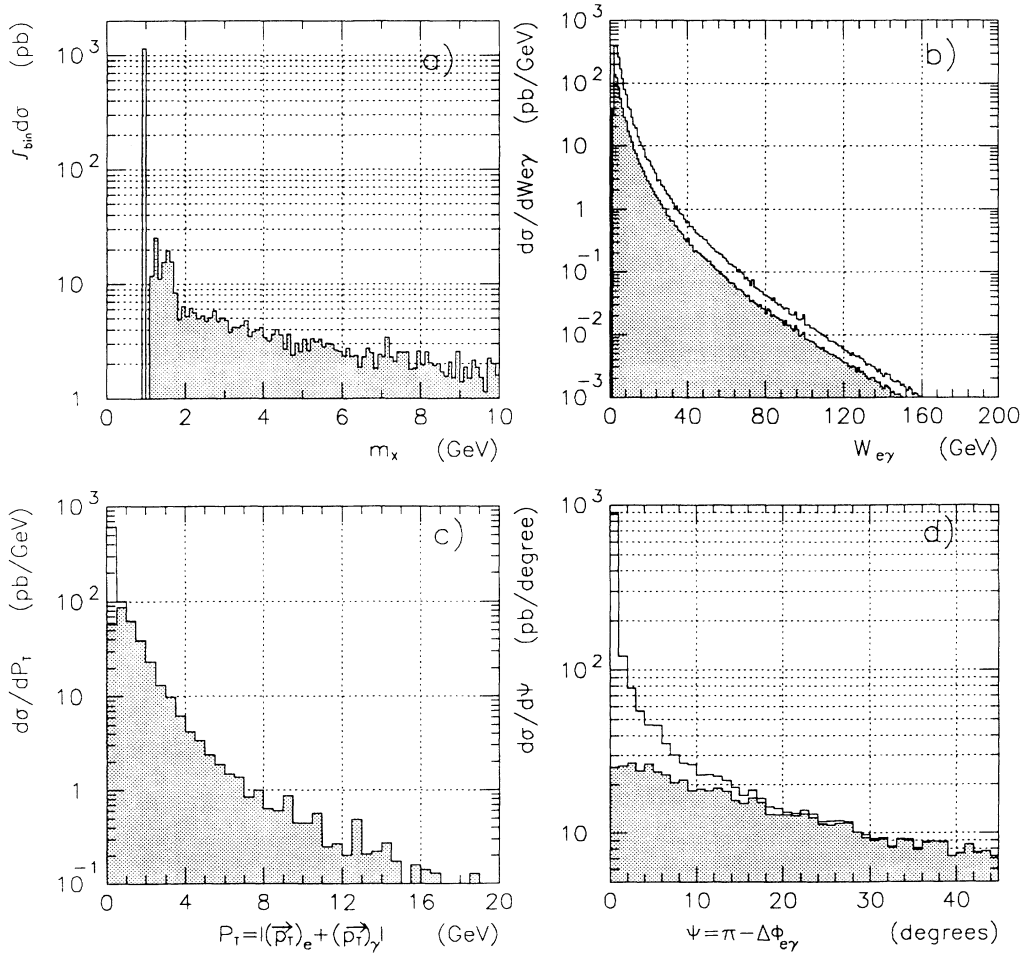

FIG. 4. Distributions of (a) hadronic mass; (b) $e\gamma$ invariant mass; (c) $e\gamma$ total transverse momentum; (d) $e\gamma$ acoplanarity, for the conditions defined in Sec. III (including acoplanarity and P_T cuts). Shaded areas represent the inelastic contribution.

III. MONTE CARLO COMPUTATIONS [8]

Because of the presence of various poles in the expressions given in Sec. II, it is practically impossible to generate at once a Monte Carlo program that would be reasonably accurate in all phase-space regions (all experimental configurations). Here we choose to generate *specific* Compton events, i.e., events with the final electron and photon nearly coplanar, each observed at finite angle (i.e., above a few degrees) in the detector; those events are dominated by quasi-real photon exchange ($q_2^2 \ll q_1^2, q_1'^2$). Our limitations of acoplanarity and polar acceptance entail $Q^2 < W^2$ and [9] $\eta \ll 1+u^*$. Therefore, in a first step, we generate the events according to an equivalent-photon-type approximation of the cross section where terms of order Q^2/W^2 (actually even of order Q/W) are neglected in formulas (7)–(10), while η is neglected as well. These are only dynamic approximations; all physical quantities (including Q^2) are generated, and the kinematics is treated exactly. The generation is performed over the experimental phase space, i.e., over the angular acceptance of the detector, defined at the beginning of the program.

In a second step the events generated are weighted by comparing, for their given parameters, the exact value of the differential cross section defined in formula (1) to the approximate one used in the first step. This allows us, in principle, to provide an exact Monte Carlo simulation over the whole phase space available. However, when we increase Q^2/W^2, the weights of the events become larger [see Fig. 2(a)]. Actually this corresponds to the fact that we are essentially moving from the "QED Compton" configuration to the "radiative correction" configuration (see our discussion in Sec. I). We must reject such large-weight events for two reasons: the first is that their statistical accuracy becomes small; the second is that we should be able, through a limited increase of the cross-section normalization, to get a weight factor smaller than 1, which would allow us to provide an output of individual (unweighted) events.

Since Q^2 is strongly correlated with, and essentially close to, the total transverse momentum squared (P_T^2) of the outgoing electron-photon system, large Q^2/W^2 values correspond to large acoplanarity angles between the electron and the photon. This is clearly shown in Fig. 2(b).

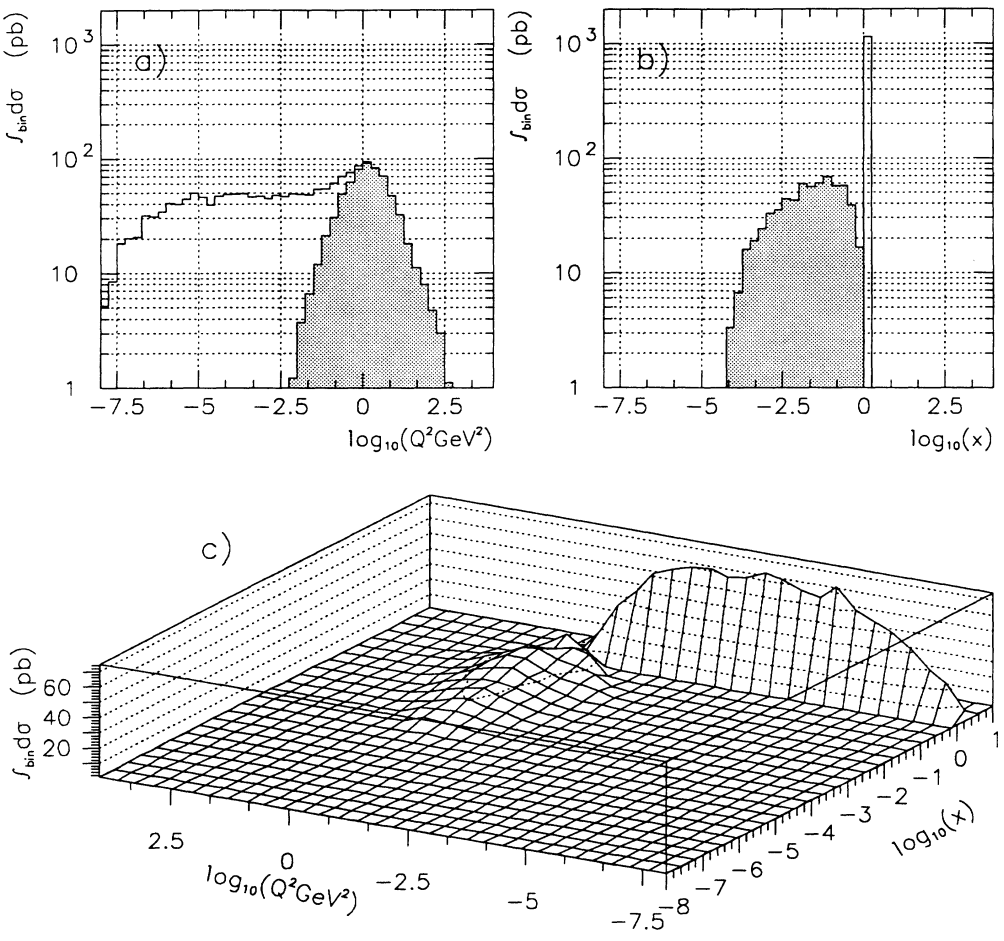

FIG. 5. (a) Q^2 distribution; (b) x distribution; (c) Q^2, x correlation, for the conditions defined in Sec. III. Shaded areas in (a) and (b) represent the inelastic contribution.

We shall thus select relatively small Q^2/W^2 values, and consequently small weights, by defining a cut on the $e\gamma$ acoplanarity angle, $\pi-\Delta\varphi<45°$ [see Fig. 2(c)], calling $\Delta\varphi$ the angle between the transverse momenta of e and γ. As mentioned in Sec. I, this cut also justifies our neglect of any contributions from diagrams where the outgoing photon is emitted at the hadron vertex.

The acoplanarity cut leads to sharp limitations on Q^2 (P_T^2) for the overwhelming contribution of small W values. However, in order to eliminate large Q^2 values even at high W (e.g., in the search for an e^*), we introduce an additional cut: $P_T<20$ GeV.

Thus restricting ourselves to relatively small Q^2, we avoid having to include any contribution from weak interactions (i.e., virtual Z exchange) in our computations. In addition we feel allowed to choose, for simplicity, scale-invariant expressions of the photon's electromagnetic structure function, as, for instance [10],

$$F_2^{\gamma}(x)=35/32\sqrt{x}\,(1-x)^3+0.2(1-x)^7\ . \tag{21}$$

Radiative corrections to the lowest-order diagrams of Fig. 1 are affecting the cross section of the Compton process, as well as the distributions of various parameters. The most significant contribution proceeds from radiation emitted by the incident electron (Fig. 3). We take that contribution into account, using the so-called peaking approximation; that procedure is justified by the fact that the radiated photon and the scattered one are essentially emitted at different angles, and thus can be distinguished, so that interference terms are suppressed. Actually, we introduce an energy loss of the initial electron according to a probability law given by the semiclassical formula [11]

$$dP(k)=\beta\cdot k^{\beta-1}(1-k+k^2/2)dk\ , \tag{22}$$

with

$$\beta=\frac{2\alpha}{\pi}\ln\left[\frac{2E}{m_e}-\frac{1}{2}\right] \tag{23}$$

and defining $k=E_\gamma/E$ where E_γ is the radiated energy

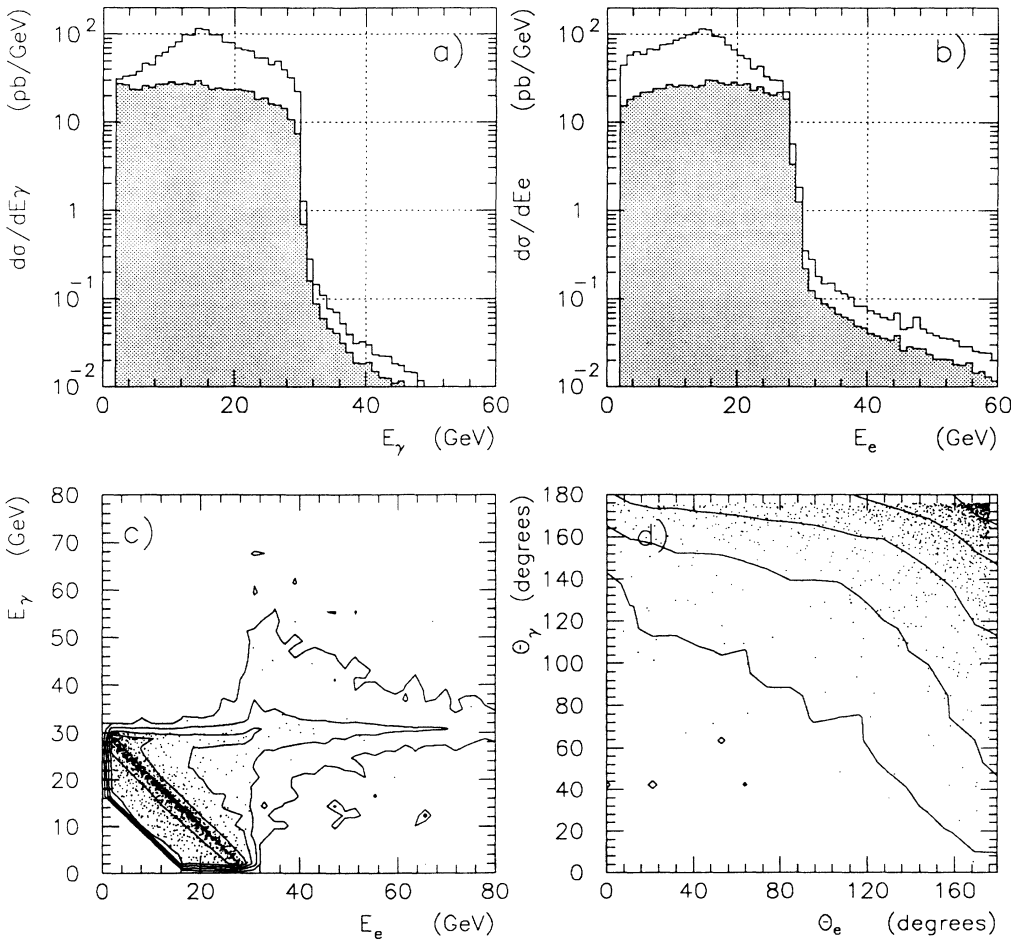

FIG. 6. Energy distribution of the (a) outgoing photon and (b) outgoing electron, and (c) energy correlation and (d) angular correlation between outgoing photon and electron, for the conditions defined in Sec. III. Shaded areas in (a) and (b) represent the inelastic contribution. In (c) and (d) the solid lines are level curves representing successive orders of magnitude of $d^2\sigma/dE_\gamma dE_e(d^2\sigma/d\theta_\gamma d\theta_e)$.

and E the energy of the electron beam.

Note that the hard-photon tail of the radiated spectrum has a low emission probability, but on the other hand it leads to smaller values of W, thus involving an increase of the QED Compton cross section. In the computations the Monte Carlo simulation uses the value of the electron energy after radiation. However this leads to weighting the events, since the absolute normalization performed at the start of the program involves the nominal beam energy. It is possible to eliminate to a large extent the hard-photon tail by imposing a lower limit of the $e\gamma$ visible energy; correspondingly, such a cut is necessary and sufficient in order to eliminate large weight factors due to the radiation.

Let us make a short remark regarding the final-state hadrons. The total outgoing-hadron invariant mass is generated by our program, but we are not interested in looking at possible hadron components inside the detector. As far as the elastic contribution is concerned, the outgoing proton, anyway, does not enter the finite-angle detector.

Figures 4–7 show various predictions (distributions, correlations) regarding different parameters of the process considered, which are provided by our Monte Carlo program with the experimental assumptions (valid for HERA):

$$E_e = 30 \text{ GeV}, \quad E_p = 830 \text{ GeV},$$

$$E_{e'} + E_\gamma > 20 \text{ GeV}, \quad E_{e'}, E_\gamma > 2 \text{ GeV},$$

$$3.6° < \theta_{e'}, \ \theta_\gamma < 176°,$$

$$\pi - \Delta\varphi < 45°, \quad P_T < 20 \text{ GeV}.$$

Notice that the same assumptions were used in Fig. 2, except for the two last cuts.

Figures 4(a)–4(d) show the expected distributions of W, m_X, P_T, and $\pi - \Delta\varphi$; they are all sharply peaked towards the minimal values of those parameters.

From Figure 5(a)–5(c), which show the distributions of $\log_{10}Q^2$ and $\log_{10}x$, as well as their correlation, we conclude that the elastic contribution ($x = 1$) is dominating until $Q^2 \approx 1$ GeV^2, and that above that value only the inelastic one remains significant; however, even the latter

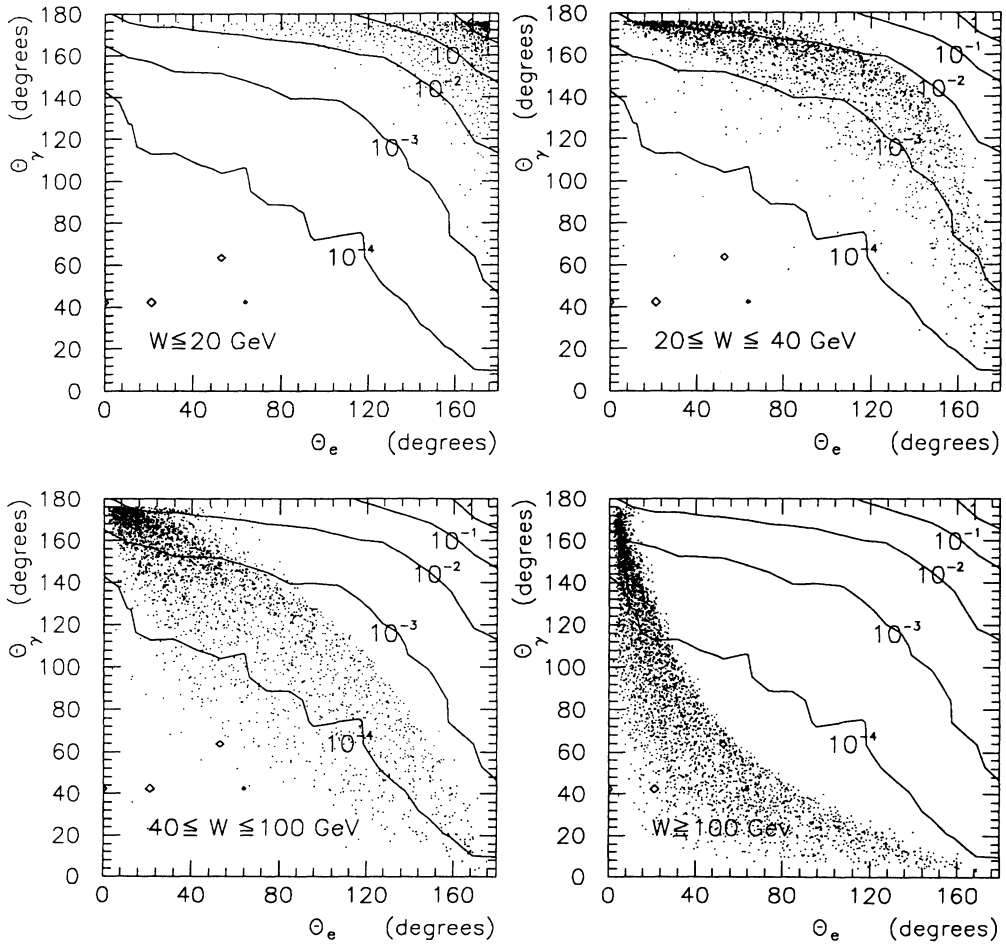

FIG. 7. Angular correlation between outgoing electron and photon in various ranges of W. The points in the scatter plots correspond to unweighted events in the indicated W ranges while the solid lines are iso-cross-section contours of $d^2\sigma/d\theta_\gamma d\theta_e$ in pb/deg^2 for all allowed values of W.

falls down very rapidly when Q^2 is further increased. Figures 6(a) and 6(b) show the distributions predicted for the outgoing photon and electron lab energies; both appear rather flat until a maximum value close to the incident-electron energy E_e. In Fig. 6(c) one observes that (i) there is a very pronounced maximum for $E_{\rm vis}$ $(\equiv E_{e'}+E_\gamma)=E_e$, (ii) there are events with lower visible energy, due to radiative corrections (we cut off for $E_{\rm vis}<20$ GeV) , and (iii) at higher $E_{\rm vis}$ the cross section decreases sharply, while $E_{e'}$ shows a somewhat longer tail than E_γ. As for Fig. 6(d), it shows that both the electron and the photon (especially the latter) tend to be emitted backwards, i.e., along the incident electron beam, in the laboratory frame. Finally, Fig. 7 shows again the θ_γ,θ_e correlation, this time in different ranges of W. One observes that the angular correlation practically determines the value of W involved. In particular the large accumulation of events for both $\theta_\gamma,\theta_e\simeq\pi$ is clearly related to the lower W range.

It appears that, with our experimental assumptions, the inelastic contribution (shaded area in the figures) represents about 36% of the integrated cross section, the latter is 1770 pb.

IV. CONCLUSION

The present study should be fit to be practically applied in the near future, especially as HERA should start running soon. In particular, it might be used (restricting oneself to measuring small acoplanarity angles, where the better known elastic contribution is by far dominating) for the determination of luminosity.

In the future we shall study corrections that should be included in our computations when the various restrictions (i.e., experimental cutoffs) introduced are relaxed to some extent: the contribution of diagrams with the photon emitted at the hadron vertex, the contribution of weak interactions; and the use of any type of proton structure function in the calculation of the inelastic contribution. In addition we shall study the hadronic final state.

ACKNOWLEDGMENTS

The authors are grateful to C. Carimalo for his advice on theoretical questions. They also wish to thank T. Carli and S. Kermiche for the implementation of the Monte Carlo program in the *CMZ* H1 standard, and for many discussions.

[1] A. Courau and P. Kessler, Phys. Rev. D **33**, 2028 (1986); see also K. Hagiwara, S. Komanya, and D. Zeppenfeld, Z. Phys. C **29**, 270 (1985).

[2] Another way of determining $f_{\gamma/p}$ would consist in measuring lepton-pair production, i.e., $ep\rightarrow eXl^+l^-$; see N. Arteaga-Romero, C. Carimalo, and P. Kessler, Z. Phys. C **52**, 289 (1991).

[3] Such a detector has been designed at HERA for measuring the machine liminosity. See L. Suszycki *et al.*, in *Proceedings of the HERA Workshop,* Hamburg, 1987, edited by R. D. Peccei (Retrolüdke, Hamburg, 1988), Vol. 2, p. 505.

[4] H. Spiesberger, in *Proceedings of the HERA Workshop* [3], Vol. 2, p. 605; J. Kripfganz, H. J. Möhring, and H. Spiesberger, Z. Phys. C **49**, 501 (1991); H. Anlauf, P. Manakos, T. Ohl, H. D. Dahmen, and T. Mannel, Report Nos. DESY 91-018 and DESY 91-100 (unpublished).

[5] C. Carimalo, P. Kessler, and J. Parisi (unpublished).

[6] See C. Carimalo, G. Cochard, P. Kessler, J. Parisi, and B. Roehner, Phys. Rev. D **10**, 1561 (1974).

[7] See, J. Drees, in *Springer Tracts in Modern Physics,* edited by G. Hohler (Springer, New York, 1971), Vol. 60, p. 107.

[8] A. Courau, HERA Note H1-187 (unpublished); A. Courau, S. Kermiche, T. Carli, and P. Kessler, HERA Note H1-207 (unpublished).

[9] The fact that the polar-acceptance cut in the lab frame also limits $\cos\theta^*$ is not absolutely obvious, but can be proven.

[10] K. Kajantje and R. Raitio, Nucl. Phys. **B139**, 72 (1978). We also used three other expressions of $F_2^p(x)$, taken from the literature; the results obtained for the inelastic contribution show variations confined between 5% and 20% (depending also on the cuts introduced).

[11] E. Etim, G. Pancheri, and B. Touschek, Nuovo Cimento **51B**, 276 (1967); G. Pancheri, *ibid.* **60A**, 321 (1969).

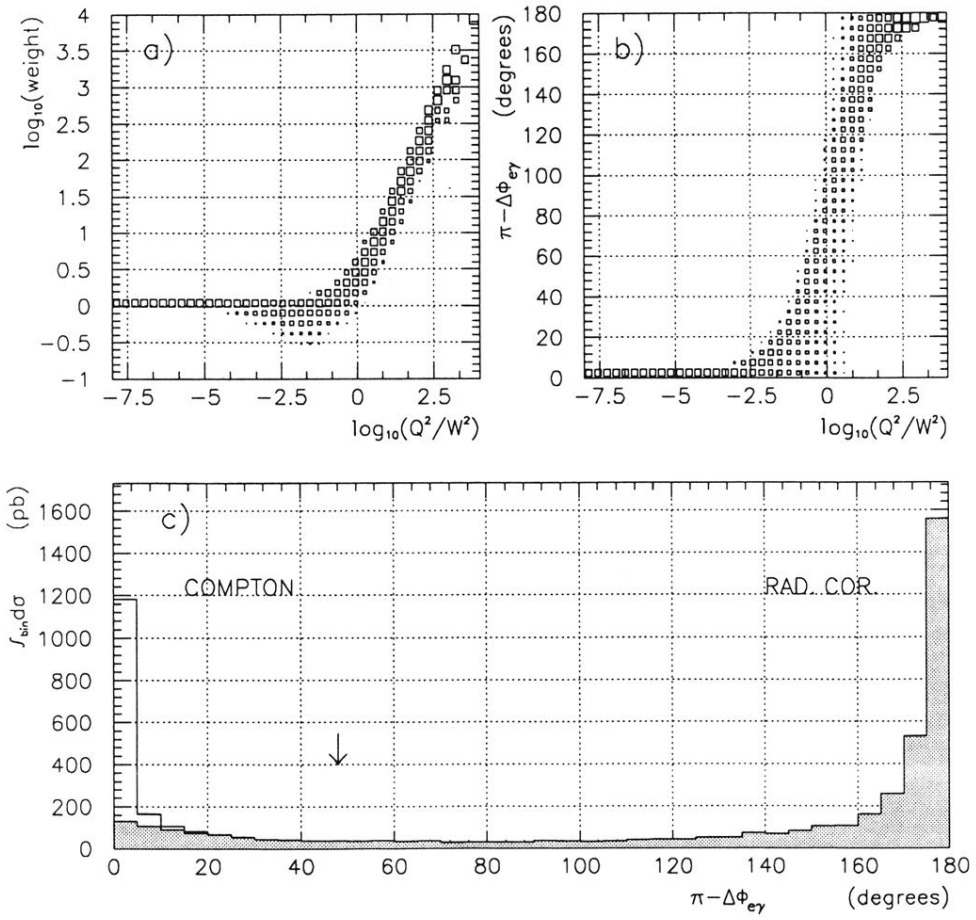

FIG. 2. (a) Correlation between Q^2/W^2 and weight (see Sec. III). (b) Correlation between Q^2/W^2 and acoplanarity angle. (c) Acoplanarity distribution; the shaded area represents the inelastic contribution. Those figures show weighted distributions computed for HERA conditions (see Sec. III) before introducing acoplanarity and P_T cuts.

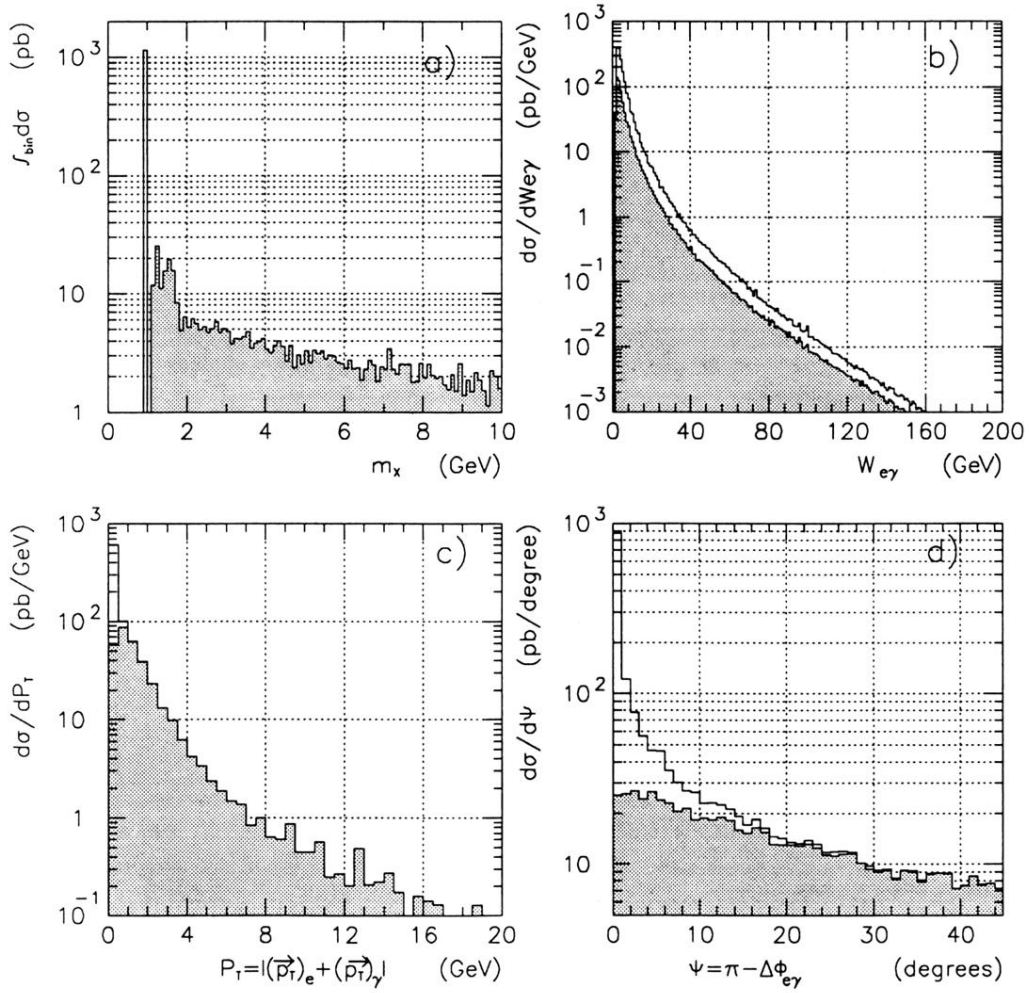

FIG. 4. Distributions of (a) hadronic mass; (b) $e\gamma$ invariant mass; (c) $e\gamma$ total transverse momentum; (d) $e\gamma$ acoplanarity, for the conditions defined in Sec. III (including acoplanarity and P_T cuts). Shaded areas represent the inelastic contribution.

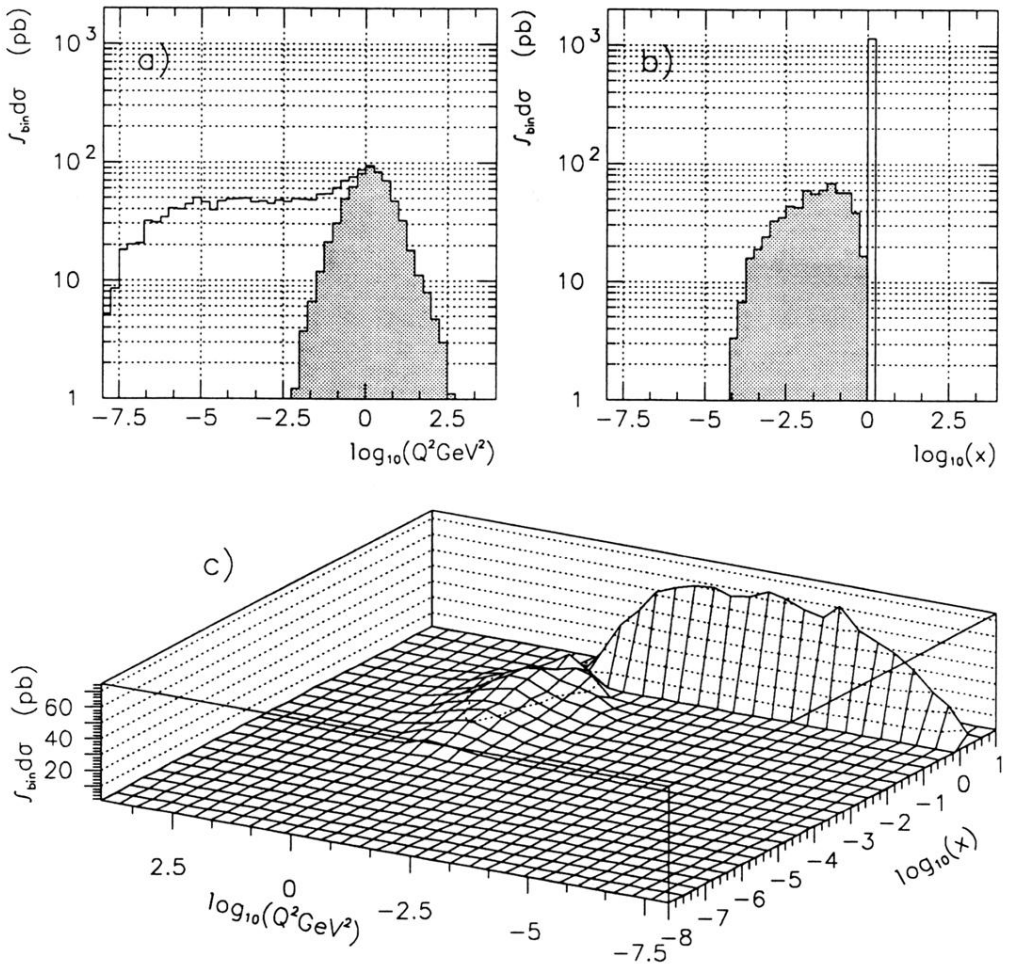

FIG. 5. (a) Q^2 distribution; (b) x distribution; (c) Q^2, x correlation, for the conditions defined in Sec. III. Shaded areas in (a) and (b) represent the inelastic contribution.

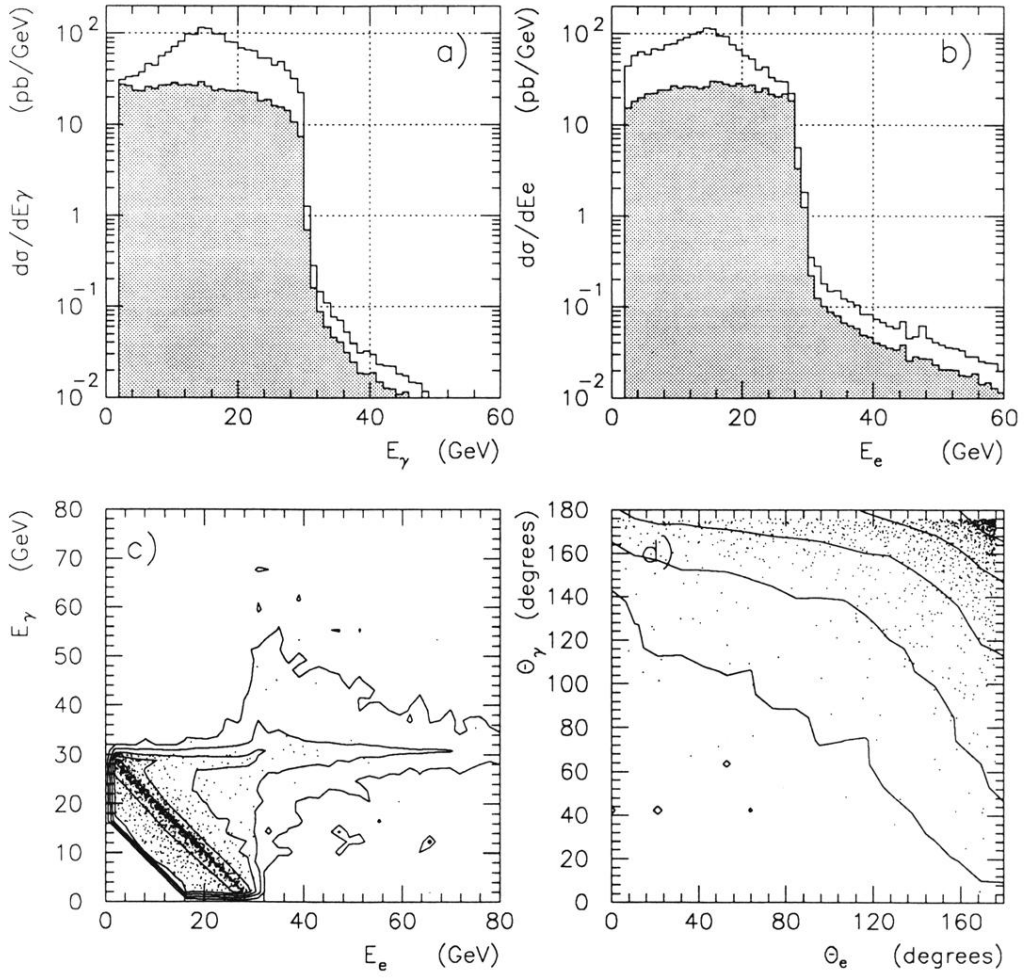

FIG. 6. Energy distribution of the (a) outgoing photon and (b) outgoing electron, and (c) energy correlation and (d) angular correlation between outgoing photon and electron, for the conditions defined in Sec. III. Shaded areas in (a) and (b) represent the inelastic contribution. In (c) and (d) the solid lines are level curves representing successive orders of magnitude of $d^2\sigma/dE_\gamma dE_e (d^2\sigma/d\theta_\gamma d\theta_e)$.